Organic Electronics 18 (2015) 44–52

Contents lists available at ScienceDirect

Organic Electronics

journal homepage: www.elsevier.com/locate/orgel

Electron injection barrier and energy-level alignment at the Au/PDI8-CN_2 interface via current–voltage measurements and ballistic emission microscopy

R. Buzio [a,*], A. Gerbi [a], D. Marrè [a,b], M. Barra [c], A. Cassinese [c]

[a] CNR-SPIN Institute for Superconductors, Innovative Materials and Devices, C.so Perrone 24, 16152 Genova, Italy
[b] Physics Department, University of Genova, Via Dodecaneso 33, 16146 Genova, Italy
[c] CNR-SPIN and Physics Department, University of Naples Federico II, Piazzale Tecchio, 80125 Napoli, Italy

ARTICLE INFO

Article history:
Received 22 October 2014
Received in revised form 31 December 2014
Accepted 2 January 2015
Available online 9 January 2015

Keywords:
Perylene diimide
Gold–organic interface
Electron injection barrier
Band alignment
Current–voltage measurements
Ballistic electron emission microscopy (BEEM)

ABSTRACT

We probe electron transport across the Au/organic interface based on oriented thin films of the high-performance *n*-type perylene diimide semiconductor PDI8-CN_2. To this purpose, we prepared organic-on-inorganic Schottky diodes, with Au directly evaporated onto PDI8-CN_2 grown on *n*-Si. Temperature-dependent current–voltage characteristics and complementary ballistic electron emission microscopy studies reveal that rectification at the Au/PDI8-CN_2 interface is controlled by a spatially inhomogeneous injection barrier, that varies on a length scale of tens of nanometers according to a Gaussian distribution with mean value ~0.94 eV and standard deviation ~100 meV. The former gradually shifts to ~1.04 eV on increasing PDI8-CN_2 thickness from 5 nm to 50 nm. Experimental evidences and general arguments further allow to establish the energetics at the Au/PDI8-CN_2 interface. Our work indicates injection-limited current flow in PDI8-CN_2-based devices with evaporated Au electrodes. Furthermore, it suggests chemical reactivity of PDI8-CN_2 with both Au and Si, driven by the lateral isocyano groups.

1. Introduction

Perylene diimide derivatives are among the most interesting *n*-type organic semiconductors because of their relatively strong electron affinities and the tailoring of the charge-transport properties upon changing the substituents on the imide N atoms or on the perylene backbone [1,2]. Hence, owing to their chemical and electronic stability in air and the tendency to form ordered layers, these molecules represent promising candidates for the development of high-mobility, highly performing devices such as field-effect transistors (OFETs).

Hereafter, we focus on the archetypical N,N′-bis(*n*-ctyl)-x:y,dicyanoperylene-3,4:9,10 bis(dicarboximide) (PDI8-CN_2), a perylene derivative functionalized with the insertion of two cyano groups directly bound to the aromatic core [1]. The presence of the electron-withdrawing cyano groups was demonstrated to significantly lower the energetic position of the lowest unoccupied molecular orbital (LUMO), thereby facilitating the electron injection from Au contacts and making the electron transport through these molecules quite insensitive to oxidative charge trapping processes related to ambient gases (i.e. O_2 and H_2O) action [1]. Nowadays, *n*-type organic transistors based on PDI8-CN_2 films display electron mobility values usually ranging between 0.01 and 0.1 $cm^2/V\,s$ being limited, in many cases, by residual contact resistances [3] where the electrons injection barrier at the Au/PDI8-CN_2 interface

* Corresponding author. Tel.: +39 010 6598 731.
E-mail address: renato.buzio@spin.cnr.it (R. Buzio).

http://dx.doi.org/10.1016/j.orgel.2015.01.007
1566-1199/

plays a major role. Hence, it is crucial to assess the size of this barrier and the practical factors that influence it, in order to gain in-depth understanding of contact effects and support strategies to improve charge injection at low voltages. Determination of the electronic barrier height also allows to model the operational response of devices in a more comprehensive way, i.e. by including the role of contacts and treating the complex interplay between injection-limited and space-charge-limited current flow [4,5]. These aspects are also particularly relevant to study charge transport in organic devices comprising single molecules and nanostructures, which performance is well known to be critically impacted by contacts contributions. So far, systematic analysis of contact resistances in OFETs performed with the transmission-line method agree with the presence of a Schottky–Mott barrier of ~0.8 eV at the Au/PDI8-CN_2 interface [3]. However, this strategy represents a highly indirect experimental approach for estimating the metal/organic barrier. Furthermore, it mostly focused on the analysis of the so-called bottom-contact configuration, where the organic film is deposited directly onto the electrode metallic surface. In the present paper we follow a different approach, by fabricating organic-on-inorganic Au/PDI8-CN_2/*n*-Si vertical diodes and exploring the related electron injection barrier at the Au/PDI8-CN_2 interface. Devices are studied by complementary electrical techniques, namely current–voltage–temperature (*I*–*V*–*T*) measurements and ballistic electron emission microscopy (BEEM). Conventional *I*–*V*–*T* curves represent an established methodology to investigate organically modified contact barrier diodes and examine electron transport across heterogeneous interfaces [6–8]. Additionally, we exploit BEEM to directly measure the electron injection barrier at the buried metal/organic interface [9–13]. We find that the Au/PDI8-CN_2 interface behaves as a spatially inhomogeneous Schottky barrier fluctuating on a length scale of tens of nanometers. We quantify the average electron injection barrier as well as the barriers spread, achieving a consistent description of the energy-level alignment at the metal/organic interface. Molecular orientational disorder and reactivity of the cyano groups toward Au are proposed to be the main reasons for the inherent interfacial inhomogeneity.

2. Experimental

Schottky junctions were prepared by vapor depositing PDI8-CN_2 (Polyera ActivInk N1200 by Polyera US) on hydrogen-terminated Si(100) (H-Si) substrates ($10 \times 5 \times 0.5$ mm^3, *n*-type, 1–10 Ohm cm, wet etching in aqueous solution with dilute 5% HF) in vacuum (base pressure $<10^{-8}$ mbar, deposition rate 1 nm/min, $T_{substrate}$ = 100 °C) [14]. The nominal thickness d_{PDI} was calibrated with a quartz crystal microbalance and is used below to label the different specimens. Top-contact Au electrodes of ~10 nm thickness were thermally evaporated *ex situ* onto the organic layer using a shadow mask (area 1.8 mm^2). Details on Si Ohmic back-contact and Au grounding are reported elsewhere [15,16]. Fig. 1 shows a schematic diagram of the fabricated devices.

The morphology of the PDI8-CN_2 films was characterized by Atomic Force Microscopy AFM (Solver P47-PRO by NT-MDT, Russia) operated in tapping-mode in air (probes Olympus AC160TS).

Ballistic emission microscopy BEEM was performed under ultra-high-vacuum UHV conditions (base pressure 5×10^{-10} mbar) using a commercial Scanning Tunneling Microscope STM (LT-STM by Omicron Nanotechnology GmbH Germany) equipped with an additional low-noise variable-gain current amplifier (custom DLPCA-200 by FEMTO GmbH Germany). In BEEM, a STM tip at bias V_T injects ballistic electrons into a thin metal overlay at a constant tunneling current I_{Tun} (Fig. 1). If the electrons energy overcomes the buried energy barrier formed between the metal and the semiconducting substrate, a current I_{BEEM} is transmitted across the sample and collected through the backside Ohmic contact [11,12,17]. The barrier height is then defined by the onset of the collector current in I_{BEEM} vs V_T spectra. Unless otherwise specified, the STM tip (electrochemically etched W) was negatively biased with respect to the grounded Au film, meaning electron transport occurs in the direction of STM tip to metal and semiconductor. For the acquisition of each BEEM spectrum the tip voltage V_T was ramped under feedback control, in this way keeping the tunneling current I_{Tun} constant. Data at each bias voltage was obtained by averaging 4096 samples. A typical spectrum consisted of 600 data points and was acquired in ~1 min.

Complementary *I*–*V*–*T* characteristics were measured under dark in the STM chamber, by replacing the BEEM current amplifier with a Keithley 6430 sub-femtoamp sourcemeter. The bias voltage was swept with a delay time of 2 s per 10 mV step.

3. Results and discussion

3.1. Morphology of PDI8-CN_2 thin films on H-Si

Optimized depositions of PDI8-CN_2 on SiO_2 attest the formation of *c*-axis oriented, homogeneous and molecularly-smooth thin films that exhibit a quasi two-dimensional (2D) layer-by-layer growth [14,18]. Here, we show that the growth mode changes for H-Si substrates. In Fig. 2, indeed, we report representative AFM topographies of polycrystalline PDI8-CN_2 films on H-Si. Ultrathin films consist of connected, three-dimensional (3D) domains, exhibiting a layered structure made of large, monomolecular terraces (Fig. 2a). Magnification of the individual domains demonstrates that they originate from a spiral growth around screw or half-loop dislocations (Fig. 2b). Elongated terraces are clearly visible – as generally observed for other perylene derivatives – and reflect the anisotropic growth driven by the strong anisotropy of the in-plane *ab* unit cell (a = 5.028 Å, b = 8.930 Å) [18]. By inspecting individual scan lines and height histograms of stepped regions, we estimated a terrace step of 2.0 ± 0.5 nm (Fig. 2c). This value is in good accordance with previous studies and agrees with the fact that the longer lattice parameter of the PDI8-CN_2 triclinic unit cell (c = 19.944 Å) is out of the plane. In other words, the

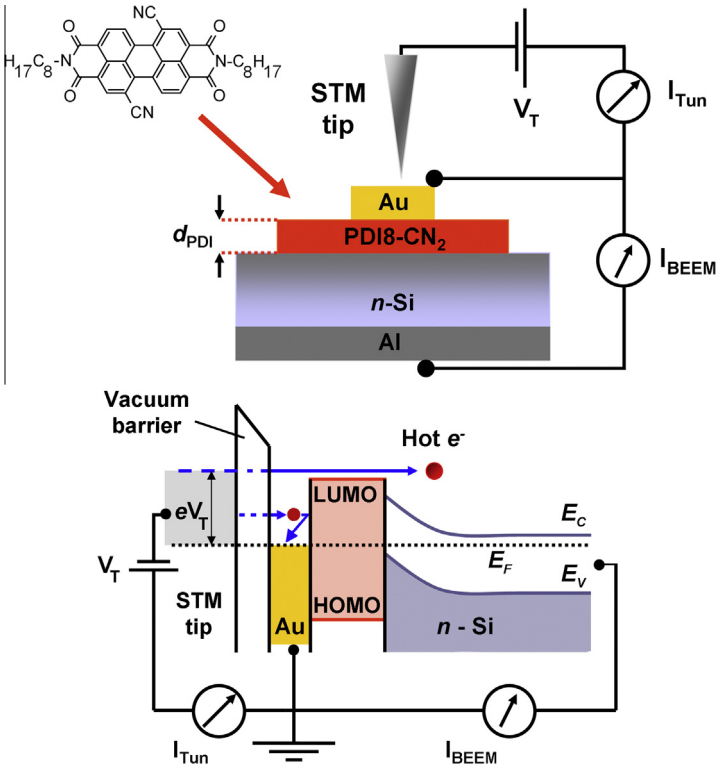

Fig. 1. (Top) Schematic diagram of the Au/PDI8-CN_2/*n*-Si contact barrier diode and the experimental set-up for BEEM measurements. (Bottom) Energy band diagram showing the conventional BEEM pathway for hot-electrons injection from the STM tip. Carriers with energy above the local interface barrier height are transmitted across the unbiased heterostructure and collected by the *n*-Si substrate, thus contributing to I_{BEEM}.

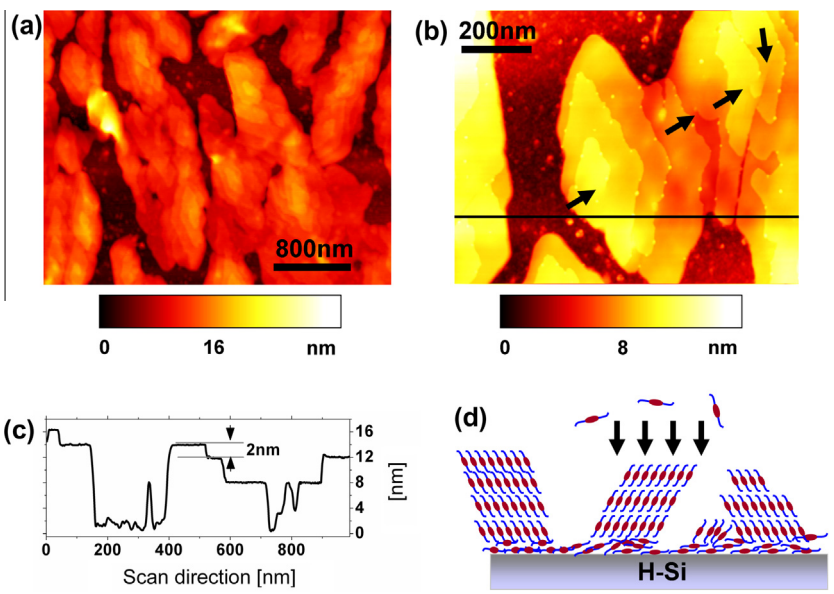

Fig. 2. (a) AFM image of a PDI8-CN_2 film on H-Si (d_{PDI} = 10 nm). Elongated 3D structures, formed by stacks of monomolecular layers, are clearly resolved. (b) AFM magnification of individual domains. The 3D spiral growth proceeds around screw or half-loop dislocations (a few cores highlighted by black arrows). Crystalline domains coexist with regions covered by nanometric globular protrusions. (c) The scan line from the topography in (b) reveals a quantized height, due to edge-on arrangement of molecules. (d) Cartoon of the growth mode: oriented domains self-assemble onto a disordered layer of flat-lying molecules.

molecules are oriented with their long inertial axis almost normal to the substrate surface (edge-on configuration) and the π–π overlap is in the substrate plane. The fact that the molecular arrangement within the crystalline domains is analogous to that reported for the bulk phase and for PDI8-CN_2 films on SiO_2 is attributed to the presence of the CN groups, that impose geometrically stiff intermolecular interactions [18]. AFM also revealed that the 3D domains laterally expand and coalesce via the spiral growth, until a continuous surface morphology emerges for $d_{PDI} > 30$ nm (not shown).

Of particular relevance for what follows are the nature and properties of those portions of the Si substrate covered by small globular protrusions of lateral size 20–50 nm and height ~1 nm (Fig. 2b). Such regions might correspond to a phase of flat-lying molecules forming a disordered, molecularly-thin wetting layer [3,19]. Beside AFM topographies, other arguments support this conclusion. Some of us recently reported that PDI8-CN_2 on SiO_2 undergoes a continuous transition from a 2D layer-by-layer growth to 3D spiral growth on increasing film thickness [20]. In the present case, ultrathin films already evolve according to the spiral growth, thus the 2D → 3D transition on H-Si possibly takes place at low coverage, after completion of a molecularly-thin layer. Moreover, model perylene derivatives form spiral islands on bare Si after completion of a disordered wetting layer that passivates dangling bonds [21]. Likewise, for PDI8-CN_2 on H-Si, formation of an initial layer might be assisted by a strong coupling with the substrate caused by the CN groups. These are known to covalently bind to H-Si by anodic grafting [22]. They might also react with Si at defect sites of the passivating hydrogen layer through cycloaddition [23]. Importantly, a limited number of chemisorbed molecules (~20%) is sufficient for the formation of the initial layer [21,24]. Further indications for the existence of a PDI8-CN_2 wetting layer arise from *I–V–T* characteristics and BEEM experiments, and are discussed below. A cartoon showing the suggested growth mode is reported in Fig. 2d.

3.2. I–V–T characteristics of the Au/PDI8-CN_2/n-Si diodes

The room temperature *I–V* characteristics of Au/PDI8-CN_2/*n*-Si diodes are shown in Fig. 3a as a function of thickness d_{PDI}. All devices rectify with polarity consistent with the Si carrier type. Importantly, *I–V* curves deviate from the Au/*n*-Si reference data in the low bias regime, confirming that the organic layers are not shorted electrically by direct deposition of Au [25]. For reverse biases and forward biases below ~0.4 V a behavior typical of Thermionic Emission (TE) is observed. For applied voltages larger than 0.4 V, the *I–V* curves depart from exponential, being affected by the transport properties of the organic material and series resistance. Least square fits to the linear part of the characteristics with the TE equation, $J = A^* T^2 \exp(-\phi_B/k_B T) \exp(qV/nk_B T)$, provided the effective barrier height ϕ_B and ideality factor n as fitting parameters. A Richardson constant $A^* = 112$ A cm^{-2} K^{-2} was used [6,26]. Fig. 3b shows that ϕ_B monotonically increases from 0.69 eV to 0.82 eV when d_{PDI} changes from 5 nm to 50 nm, whereas n remains higher then unity ($\geqslant 2$). Notably, an abrupt change of transport takes place for $d_{PDI} = 5$ nm, therefore molecules affect majority bands line-up already in form of ultrathin layers sandwiched between Au and *n*-Si. This transition also indicates that the portions of H-Si substrate which are covered by small globular protrusions (Fig. 2b)

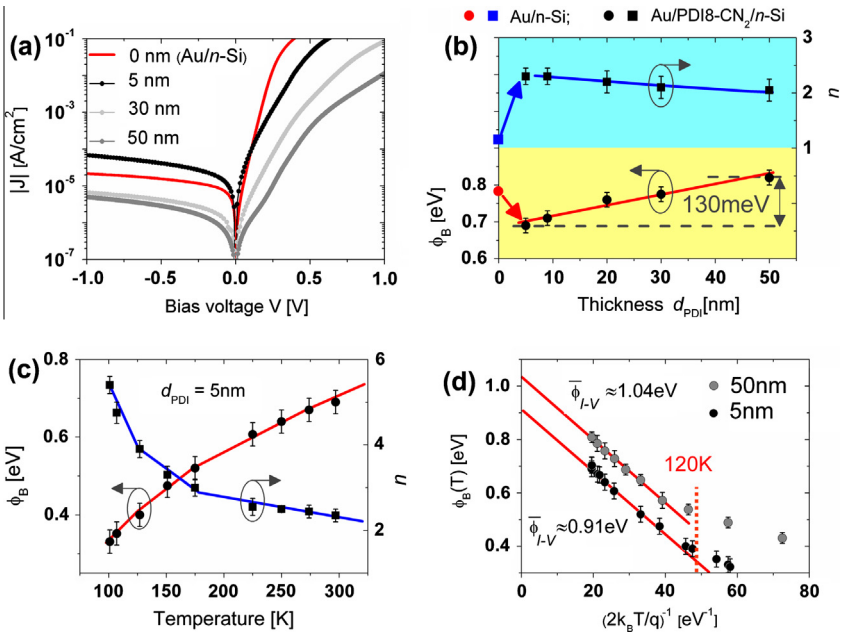

Fig. 3. (a) Room temperature *I–V* curves measured for Au/PDI8-CN_2/*n*-Si diodes. Forward bias is with positive voltage applied to Au. Current density strongly depends on the organic thickness. (b) The effective barrier height ϕ_B and ideality factor n as a function of d_{PDI}. (c) The temperature-dependence of ϕ_B and n indicates spatial inhomogeneity with a distribution of barriers. (d) Plot of $\phi_B(T)$ vs $1/T$. Interpolation is done with the Gaussian fluctuation model (see text).

do not behave as intimate Au/*n*-Si junctions, which are known to give $\phi_B \approx 0.8$ eV and $n \approx 1$ [27,28]. On the contrary, as observed in the previous section, a wetting layer of flat-lying molecules very likely separates Au and Si (see Fig. 2d).

The estimated ϕ_B and n values are close to previous reports on Au/perylene derivatives/*n*-Si diodes [6,26,29]. Idealities $n > 1$ often appear for metal/organic/Si devices and can be related to several effects, including spatially inhomogeneous Schottky contacts, bias voltage dependence of the barrier height, image-force lowering and interface states. We claim that spatial inhomogeneity is playing the major role in the present case. This stems from the TE analysis of *I–V–T* characteristics (representative *I–V–T* curves are shown in Supplementary Material). Fig. 3c shows that the junction response strongly depends on temperature *T*, since a simultaneous lowering of ϕ_B and increase of n take place on decreasing *T*. Such trend is observed for specimens with different d_{PDI} values and represents a signature for the existence of a distribution of barriers [30,31].

In the framework of a potential fluctuations model assuming Gaussian variations of the local barrier height [30], the mean value $\bar{\phi}_{I-V}$ and standard deviation σ of the distribution are obtained by linear regression of the experimental $\phi_B(T)$ vs $1/T$ plot with the theoretical relationship $\phi_B(T) = \bar{\phi}_{I-V} - \sigma^2 q/2k_BT$. Fig. 3d shows that experimental data are satisfyingly fitted with a straight line over a broad temperature range ($120\ \text{K} \leqslant T \leqslant 300\ \text{K}$), with best fit parameters $\bar{\phi}_{I-V} = (0.91 \pm 0.01)$ eV, $\sigma \cong 110$ meV for $d_{PDI} = 5$ nm and $\bar{\phi}_{I-V} = (1.04 \pm 0.01)$ eV, $\sigma \cong 110$ meV for $d_{PDI} = 50$ nm. Comparison with the distribution of bare, abrupt Au/*n*-Si junctions [27,28] ($\bar{\phi}^{Au/Si} = 0.83$—$0.87$ eV, $\sigma^{Au/Si} = 20$—80 meV) demonstrates that the insertion of the PDI8-CN_2 layer shifts the mean barrier height toward higher energies and enhances the distribution width. A similar trend was reported for other hybrid organic–inorganic contacts [8], including perylene-based diodes [26,29,32]. Given the inhomogeneous nature of the fabricated devices, it follows that the current across the Au/PDI8-CN_2/*n*-Si diodes preferentially flows through the local barrier minima, corresponding to the low-barriers tail of the Gaussian distribution.

3.3. Ballistic electron transport across the Au/PDI8-CN_2/n-Si diodes

In view of the inhomogeneous nature of the Schottky junction highlighted by *I–V–T* analysis, we further explored the distribution of barriers via BEEM spectroscopy. In this work BEEM experiments were carried out at ~120 K to increase the signal-to-noise ratio against the poor ballistic transmittance (see below), while remaining in a range of temperatures where the potential fluctuations model holds (see Fig. 3d). Furthermore, we enhanced ballistic injection using a relatively high I_{Tun}, usually from 20 nA to 80 nA. About one thousand spectra, arranged in square grids of $150 \times 150\ \text{nm}^2$ area, were acquired at different locations of the top Au electrode. In fact, we found that the repeated acquisition of high-density grids at the same spot caused modifications of the Au morphology and of the interfacial properties (see Supplementary Material). Therefore, the surface locations probed by BEEM were separated by hundreds of nanometers ($\geqslant$500 nm) and each grid (typically 8×8 spectra with spacing ~19 nm) was acquired at the same point only once, to reduce to a minimum the degradation of the surface and of the buried interfaces. In Fig. 4a we report a representative raw spectrum, with Schottky barrier threshold $V_{th,SB} \sim -0.90$ V and hot electron injection efficiency $I_{BEEM}/I_{Tun} \sim 1 \times 10^{-6}$ at 0.3 eV above $V_{th,SB}$. Notably, a second onset of the collector current exists at $V_{th,PC} \sim -1.26$ V, which is slightly larger than the Si band gap at 120 K (~1.16 V). As discussed by Heller et al. [33], the portions of spectra above $V_{th,PC}$ are due to STM-induced photocurrent (STM-PC) in Si rather than to a real injection of hot electrons. On the contrary, the *true* ballistic signal concerns spectral regions immediately above the first onset $V_{th,SB}$. Analysis of neighbor spectra within individual grids revealed a dramatic variation of BEEM efficiency on the nanoscale. In detail, spectra with efficiency $>10^{-5}$ were rarely detected, being ~1% of the totally acquired data. Spectra with efficiency 10^{-6} (as in Fig. 4a) were ~20% and were recorded at isolated nanosized domains (see additional BEEM data reported in the Supplementary Material). They appeared with frequency of 2–10 per grid and were distributed over the Au surface without apparent correlation with the buried organic structures (e.g. crystalline domains or grain boundaries). The majority of the spectra however did not show the ballistic threshold $V_{th,SB}$ up to the photocurrent onset $V_{th,PC}$. Such behavior attested the significant attenuation experienced by hot electrons crossing PDI8-CN_2 and their enhanced scattering at the organic/inorganic interfaces. Earlier reports also show that the insertion of organic layers at the Au/*n*-Si interface decreases the BEEM efficiency by orders of magnitude until a negligible transmittance occurs for a layer thickness of a few nanometers [12,34]. For such reasons we restricted BEEM experiments to the samples with the thinnest interlayer ($d_{PDI} = 5$ nm).

We investigated the Schottky barrier inhomogeneity by fitting each spectrum (clearly showing the Schottky onset, as in Fig. 4a) with the Bell and Kaiser (BK) phase space model, i.e. $I_{BEEM}/I_{Tun} = R(eV_T - eV_{th,SB})^2/eV_T$ (e elementary charge, fitting range $-0.3\ \text{V} < V_T < -1.2\ \text{V}$), in order to extract the local value of Schottky barrier height $eV_{th,SB}$ and transmission attenuation factor *R*.

Fig. 4b shows the histogram of the barriers extracted from a selected ensemble of 220 spectra. One can observe two energetically-distinct contributions, respectively a Gaussian distribution centered at ~0.94 eV and a broad "shoulder" of smaller barriers roughly extending from 0.5 eV to 0.8 eV. The spread of barriers largely overcomes that of Au/*n*-Si bare interface [12,27,28] and points toward an inherent interfacial inhomogeneity induced by the presence of the PDI8-CN_2 molecules. As discussed below, the Gaussian distribution originates from the hot electrons injection across the buried Au/PDI8-CN_2 interface. On the other side, the tail of lower barriers regards the PDI8-CN_2/Si interface, which is detected because of quantum tunneling of ballistic electrons from Au into *n*-Si below the LUMO of PDI8-CN_2 [12]. Under this hypothesis, we ensemble averaged the spectra contributing to the

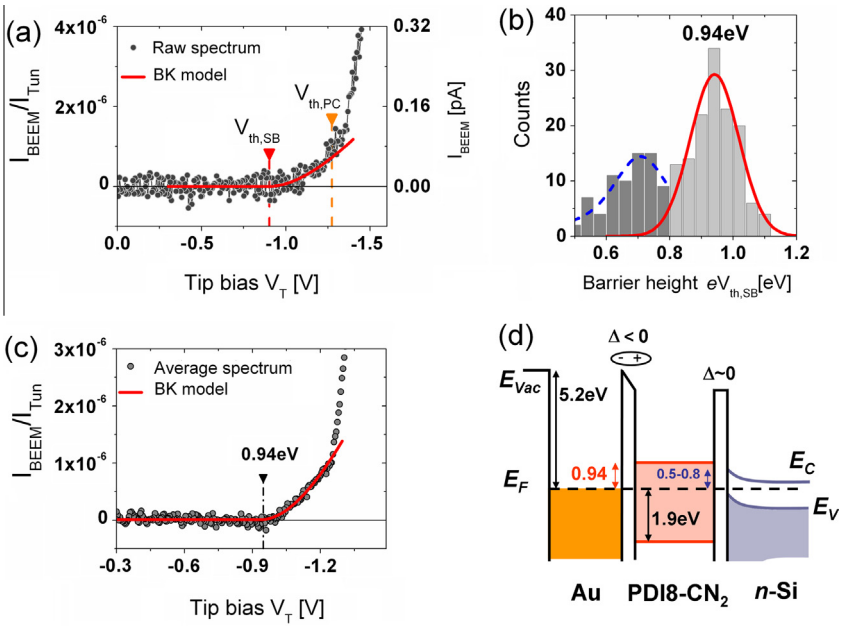

Fig. 4. (a) Raw BEEM spectrum with two onsets, related to ballistic injection and STM-PC respectively (I_{Tun} = 80 nA). (b) Histogram of the local barrier heights extracted from 220 individual spectra. Red curve is a Gaussian fit above 0.8 eV. Blue dash curve is a guide to eye. (c) Average spectrum calculated from a subsets of 60 curves corresponding to the light gray histogram in (b). (d) Heterojunction energetic alignment at zero bias. E_F is the Fermi energy of the sample, E_V and E_C are the valence and conduction bands of Si, respectively. Red and blue values are from BEEM experiments (units eV). (For interpretation of the references to colour in this figure legend, the reader is referred to the web version of this article.)

Gaussian distribution and fitted the average plot with the BK model. In this way, we obtained the average barrier $\bar{\phi}_{BEEM} = (0.94 \pm 0.05)$ eV and the average transmission attenuation factor $\bar{R} \cong 1.4 \times 10^{-5}$ eV^{-1} (Fig. 4c). Importantly $\bar{\phi}_{BEEM}$ agrees with $\bar{\phi}_{I-V} \cong 0.91$ eV extrapolated from *I–V–T* curves, therefore the two techniques coherently estimate the average barrier height for d_{PDI} = 5 nm. We note that the statistical spread of the histogram in Fig. 4b) originates from two distinct contributions, namely the lateral variations of the barrier height at the buried interfaces and the measurement noise [28]. A careful analysis indicates that experimental uncertainty contributes to the spread with ~70–80 meV so that the actual barrier inhomogeneity at the Au/PDI8-CN_2 interface is reduced from the measured distribution to ~160 meV (full-width-at-half-maximum) and at the PDI8-CN_2/Si interface to ~180 meV. Such values are likely affected, to some extent, by the screening properties of the semiconductors PDI8-CN_2 and *n*-Si [27]. By combining BEEM and *I–V–T* analysis one gets ~100 meV as a reasonable estimate for the standard deviation of the barrier spread at the Au/PDI8-CN_2 interface (see Supplementary Material). Finally, it is important to remember that due to the spotlike transparency of the interfaces, the spectra contributing to the histogram of Fig. 4b) are randomly distributed within the grids, with typical in-plane distance ranging from 20 to 60 nm (i.e. from one to more grid steps). Therefore, BEEM spectroscopy reveals fluctuations of the barrier height on a length scale of tens of nanometers. Furthermore, it gives insight on the heterojunction energy-level alignment at zero bias, as discussed hereafter.

3.4. Electron injection barrier and energy-level alignment at the Au/PDI8-CN_2 interface

We assume that $\bar{\phi}_{BEEM} \cong 0.94$ eV should be associated to the electron injection barrier at the Au/PDI8-CN_2 interface, i.e. the LUMO should be on the average 0.94 eV above the Fermi energy of Au. On the other hand, the "shoulder" of barriers between 0.5 eV and 0.8 eV should be related to the position of the Si conduction band edge at the PDI8-CN_2/*n*-Si interface. The corresponding band diagram, reported in Fig. 4d, is supported by different arguments. First, the LUMO position is consistent with predictions based on literature values for the constituent materials. Taking $I = 7.1$ eV [35] and $E_g^{elec} = 2.9$ eV, respectively for the ionization energy and transport gap of PDI8-CN_2 ($E_g^{elec} \approx E_g^{opt} + 0.5$ eV [36,37] and $E_g^{opt} = 2.4$ eV [1]), and $\phi_M = 5.2$ eV for the work function of polycrystalline Au, the hole injection barrier is $\phi_B^p = I - \phi_M = 1.9$ eV and the electron injection barrier is $\phi_B^n = E_g^{elec} - \phi_B^p = 1.0$ eV. Hence, ϕ_B^n matches $\bar{\phi}_{BEEM} \cong 0.94$ eV. Recent photoelectron spectroscopy studies [38] locate the highest occupied molecular orbital (HOMO) 1.9 eV below the Fermi energy of Au – as argued above and depicted in Fig. 4d – and document the formation of a negative interfacial dipole $\Delta < 0$ at the Au/PDI8-CN_2 interface. We included this evidence in the diagram for consistency. Second, an electronic barrier of 0.5–0.8 eV at the PDI8-CN_2/*n*-Si interface is in line with the small difference of electron affinities between PDI8-CN_2 (~4.2 eV) and *n*-Si (4.05 eV) and with the fact that in such case Si Fermi level pinning gives barriers of 0.4–0.7 eV [39].

A relevant question pertains the physical origin of the spread of the measured barriers. Spatial inhomogeneity commonly emerges in organically modified diodes and can be ascribed to several reasons, as direct shorts between Au and *n*-Si across the organic layer, partial disruption of molecules as a result of direct metal evaporation, intermixing and new phases driven by chemical reactions, interfacial contamination or molecular disorder [25]. Whereas it is far from obvious to unravel the specific contributions giving rise to inhomogeneity at the Au/PDI8-CN_2 interface, experimental evidences on thin films growth (see Fig. 2) and the background literature suggest that inhomogeneity might come from tiny, local variations of the molecular orientation and packing [40], and the well known capability of the cyano groups to promote molecular chemisorption on Au [41]. Likewise, the spread of barriers at the PDI8-CN_2/*n*-Si interface (corresponding to the "shoulder" of the histogram in Fig. 4b) might originate from small fluctuations of the organic layer thickness – that modulate Si band banding through image-force lowering effects [7,12] – and the already mentioned reactivity of CN toward H-Si [22,23]. Transport data of Fig. 3d complete the picture of barrier inhomogeneity for $d_{PDI} > 5$ nm. The standard deviation σ remains the same for 5 nm- and 50 nm-thick interlayers, which further supports the assumption of prominent interfacial reactivity when depositing Au contacts onto PDI8-CN_2. On the other side, we suggest that the ~130 meV increase of the average barrier height $\bar{\phi}_{I-V}$ with film thickness likely reflects a gradual shift of the LUMO and HOMO positions toward lower binding energies, due to small changes in the molecular orientation and ordering as a function of the nominal film thickness. Indeed, thickness-dependent energy level shifts are known to occur for different organic materials, e.g. phthalocyanine [42], and have been recently observed for PDI8-CN_2 vapor deposited on Au [35].

In view of the high electron barrier values found for the Au/PDI8-CN_2 interface, between ~0.91 eV and ~1.04 eV, one can conclude that devices with top-contact architecture are injection-limited [5]. Consequently, our study further supports those efforts that aim to mitigate the metal/organic contact resistance by fabrication of bottom-contact structures with chemically-tailored electrodes [3]. In fact, chemisorbed self-assembled monolayers can reduce the metal work function through intrinsic dipoles contributions hence, as a result, better matching of the metal and LUMO levels is expected.

Further investigations with surface sensitive spectroscopic techniques are certainly required to deeply address the issue of chemical reactivity of PDI8-CN_2 with Au and Si. Despite uncertainties on its origin, the barrier inhomogeneity resolved by BEEM appears relevant to studies that challenge the fabrication and optimization of PDI8-CN_2-based nanodevices, or that quantify the intrinsic electrical characteristics of different supramolecular assemblies (e.g. microscopic fibers). The existence of nanoscale potential fluctuations at Au/PDI8-CN_2 contacts might also shed light on the large uncertainty in the transport properties typically extracted from conductive-AFM data [43].

4. Conclusions

In summary, we determined the electron injection barrier, energy-level alignment and nanoscale spatial inhomogeneity at the Au/PDI8-CN_2 interface. Hybrid heterostructures were prepared by evaporating Au electrodes directly onto oriented organic thin films grown on hydrogen-terminated *n*-Si. The room temperature *I–V* curves clearly showed rectification, together with a gradual shift of the effective Schottky barrier height from 0.69 eV to 0.82 eV on increasing the PDI8-CN_2 thickness from 5 nm to 50 nm. Refined analysis of *I–V–T* characteristics and BEEM spectra revealed that electron transport across the metal/organic interface is dominated by low-barrier patches and interfacial inhomogeneity, that occur on a length scale of tens of nanometers. In view of the affinity of cyano groups toward Au, we suggest that chemical interaction of Au with PDI8-CN_2 might strongly contribute to the observed phenomenology. Finally, we exploited experimental evidences and general arguments to extract the energetics of the metal/organic interface. The band diagram consistently incorporates *I–V–T* and BEEM data – for the LUMO position – and literature results of valence band photoemission spectroscopy – for the HOMO position. In particular, the LUMO turns out to be ~0.94 eV above the Fermi energy of Au for the case of ultrathin organic layers.

Our study highlights general features of current transport in PDI8-CN_2-based devices with evaporated Au electrodes and suggests the prominence of injection-limited current flow. The direct determination of the electron injection barrier by BEEM provides input parameters to model the operational response of very diverse devices, as light emitting diodes, OFETs and photovoltaic devices and optimize their performance.

From a different perspective, the present investigation demonstrates that the electrical properties of Au/*n*-Si Schottky diodes are effectively modified by PDI8-CN_2. We reported ~130 meV barrier height engineering at room temperature through proper tuning of the perylene thickness, with rectifying ratio $>10^3$ and current carrying capacity $>10^{-2}$ A/cm^2 at 1 V bias. Such performances, together with the ambient stability of transport, offer remarkable advantages compared to organic-on-inorganic junctions using other perylene derivatives.

Acknowledgements

We acknowledge support by the Italian MIUR through Progetto Premiale 2012 "EOS: organic electronics for advanced research instrumentation", PRIN 2010NR4MXA "OXIDE", FIRB RBAP115AYN "Oxides at the nanoscale: multifunctionality and applications".

Appendix A. Supplementary material

Supplementary data associated with this article can be found, in the online version, at http://dx.doi.org/10.1016/j.orgel.2015.01.007.

References

[1] B.A. Jones, A. Facchetti, M.R. Wasielewski, T.J. Marks, Tuning orbital energetics in arylene diimide semiconductors. materials design for ambient stability of *n*-type charge transport, J. Am. Chem. Soc. 129 (2007) 15259–15278, http://dx.doi.org/10.1021/ja075242e.

[2] J. Gao, C. Xiao, W. Jiang, Z. Wang, Cyano-substituted perylene diimides with linearly correlated LUMO levels, Org. Lett. 16 (2014) 394–397, http://dx.doi.org/10.1021/ol403250r.

[3] J. Youn, G.R. Dholakia, H. Huang, J.W. Hennek, A. Facchetti, T.J. Marks, Influence of thiol self-assembled monolayer processing on bottom-contact thin-film transistors based on *n*-type organic semiconductors, Adv. Funct. Mater. 22 (2012) 1856–1869, http://dx.doi.org/10.1002/adfm.201102312.

[4] M. Marinkovic, D. Belaineh, V. Wagner, D. Knipp, On the origin of contact resistances of organic thin film transistors, Adv. Mater. 24 (2012) 4005–4009, http://dx.doi.org/10.1002/adma.201201311.

[5] M. Gruber, F. Schürrer, K. Zojer, Relation between injection barrier and contact resistance in top-contact organic thin-film transistors, Org. Electron. 13 (2012) 1887–1899, http://dx.doi.org/10.1016/j.orgel.2012.05.009.

[6] S.R. Forrest, M.L. Kaplan, P.H. Schmidt, Organic-on-inorganic semiconductor contact barrier diodes. II. Dependence on organic film and metal contact properties, J. Appl. Phys. 56 (1984) 543, http://dx.doi.org/10.1063/1.333944.

[7] T.U. Kampen, S. Park, D.R.T. Zahn, Organic modified Schottky contacts: barrier height engineering and chemical stability, J. Vac. Sci. Technol. B Microelectron. Nanom. Struct. 21 (2003) 879, http://dx.doi.org/10.1116/1.1562636.

[8] I. Taşçıoğlu, U. Aydemir, S. Altındal, The explanation of barrier height inhomogeneities in Au/n-Si Schottky barrier diodes with organic thin interfacial layer, J. Appl. Phys. 108 (2010) 064506, http://dx.doi.org/10.1063/1.3468376.

[9] H. Haick, J.P. Pelz, T. Ligonzo, M. Ambrico, D. Cahen, W. Cai, et al., Controlling Au/n-GaAs junctions by partial molecular monolayers, Phys. Stat. Solidi 203 (2006) 3438–3451, http://dx.doi.org/10.1002/pssa.200622381.

[10] S. Özcan, J. Smoliner, T. Dienel, T. Fritz, Temperature dependent Schottky barrier height and Fermi level pinning on Au/HBC/GaAs diodes, Appl. Phys. Lett. 92 (2008) 153309, http://dx.doi.org/10.1063/1.2912062.

[11] N. Chandrasekhar, Ballistic emission microscopy studies on metal–molecule interfaces, J. Phys. Condens. Matter. 20 (2008) 374113, http://dx.doi.org/10.1088/0953-8984/20/37/374113.

[12] K.E.J. Goh, A. Bannani, C. Troadec, Imaging buried organic islands by spatially resolved ballistic electron emission spectroscopy, Nanotechnology 19 (2008) 445718, http://dx.doi.org/10.1088/0957-4484/19/44/445718.

[13] M. Gobbi, L. Pietrobon, A. Atxabal, A. Bedoya-Pinto, X. Sun, F. Golmar, et al., Determination of energy level alignment at metal/molecule interfaces by in-device electrical spectroscopy, Nat. Commun. 5 (2014) 4161, http://dx.doi.org/10.1038/ncomms5161.

[14] M. Barra, F.V. Di Girolamo, F. Chiarella, M. Salluzzo, Z. Chen, A. Facchetti, et al., Transport property and charge trap comparison for N-channel perylene diimide transistors with different air-stability, J. Phys. Chem. C 114 (2010) 20387–20393, http://dx.doi.org/10.1021/jp103555x.

[15] R. Buzio, A. Gerbi, A. Gadaleta, L. Anghinolfi, F. Bisio, E. Bellingeri, et al., Modulation of resistance switching in Au/Nb:$SrTiO_3$ Schottky junctions by ambient oxygen, Appl. Phys. Lett. 101 (2012) 243505, http://dx.doi.org/10.1063/1.4771603.

[16] A. Gerbi, R. Buzio, A. Gadaleta, L. Anghinolfi, M. Caminale, E. Bellingeri, et al., Ballistic transport at the nanometric inhomogeneities in Au/Nb:$SrTiO_3$ resistive switches, Adv. Mater. Interfaces 1 (2014) 1300057, http://dx.doi.org/10.1002/admi.201300057.

[17] C. Ventrice, V. LaBella, G. Ramaswamy, H. Yu, L. Schowalter, Measurement of hot-electron scattering processes at Au/Si(100) Schottky interfaces by temperature-dependent ballistic-electron-emission microscopy, Phys. Rev. B 53 (1996) 3952–3959, http://dx.doi.org/10.1103/PhysRevB.53.3952.

[18] F. Liscio, S. Milita, C. Albonetti, P. D'Angelo, A. Guagliardi, N. Masciocchi, et al., Structure and morphology of PDI8-CN_2 for n-type thin-film transistors, Adv. Funct. Mater. 22 (2012) 943–953, http://dx.doi.org/10.1002/adfm.201101640.

[19] F. Liscio, C. Albonetti, K. Broch, A. Shehu, S.D. Quiroga, L. Ferlauto, et al., Molecular reorganization in organic field-effect transistors and its effect on two-dimensional charge transport pathways, ACS Nano 7 (2013) 1257–1264.

[20] F. Chiarella, M. Barra, A. Cassinese, F.V. Di Girolamo, P. Maddalena, L. Santamaria, et al., Dicyanoperylene-diimide thin-film growth: a combined optical and morphological study, Appl. Phys. A 104 (2010) 39–46, http://dx.doi.org/10.1007/s00339-010-6164-4.

[21] T. Soubiron, F. Vaurette, J.P. Nys, B. Grandidier, X. Wallart, D. Stiévenard, Molecular interactions of PTCDA on Si(100), Surf. Sci. 581 (2005) 178–188, http://dx.doi.org/10.1016/j.susc.2005.02.050.

[22] M.R. Linford, C.E.D. Chidsey, Alkyl monolayers covalently bonded to silicon surfaces, J. Am. Chem. Soc. 115 (1993) 12631–12632, http://dx.doi.org/10.1021/ja00079a071.

[23] F. Tao, W.S. Sim, G.Q. Xu, M.H. Qiao, Selective binding of the cyano group in acrylonitrile adsorption on Si(100)-2 x 1, J. Am. Chem. Soc. 123 (2001) 9397–9403.

[24] G. Salvan, D.R.T. Zahn, Evidence for strong interaction of PTCDA molecules with defects on sulphur-passivated GaAs(100), Europhys. Lett. 67 (2004) 827–833, http://dx.doi.org/10.1209/epl/i2004-10116-7.

[25] R.T.W. Popoff, K.L. Kavanagh, H.-Z. Yu, Preparation of ideal molecular junctions: depositing non-invasive gold contacts on molecularly modified silicon, Nanoscale 3 (2011) 1434–1445, http://dx.doi.org/10.1039/c0nr00677g.

[26] N. Tuğluoğlu, Ö.F. Yüksel, H. Şafak, S. Karadeniz, The double Gaussian distribution of inhomogeneous barrier heights in the organic-on-inorganic Schottky devices, Phys. Stat. Solidi 209 (2012) 2313–2316, http://dx.doi.org/10.1002/pssa.201228163.

[27] H. Palm, M. Arbes, M. Schulz, Fluctuations of the Au–Si (100) Schottky barrier height, Phys. Rev. Lett. 71 (1993) 2224–2228.

[28] C. Troadec, K.E.J. Goh, Dual parameter ballistic electron emission spectroscopy analysis of inhomogeneous interfaces, J. Vac. Sci. Technol. B Microelectron. Nanom. Struct. 28 (2010) C5F1, http://dx.doi.org/10.1116/1.3428546.

[29] O.F. Yúksel, M. Kuş, N. Şimşir, H. Şafak, M. Şahin, E. Yenel, A detailed analysis of current–voltage characteristics of Au/perylene-monoimide/n-Si Schottky barrier diodes over a wide temperature range, J. Appl. Phys. 110 (2011) 024507, http://dx.doi.org/10.1063/1.3610394.

[30] J.H. Werner, H.H. Güttler, Barrier inhomogeneities at Schottky contacts, J. Appl. Phys. 69 (1991) 1522, http://dx.doi.org/10.1063/1.347243.

[31] W. Mönch, Some comments on the determination and interpretation of barrier heights of metal–semiconductor contacts, Appl. Phys. A 87 (2007) 359–366, http://dx.doi.org/10.1007/s00339-007-3925-9.

[32] Ö.F. Yüksel, N. Tuğluoğlu, H. Şafak, Z. Nalçacıgil, M. Kuş, S. Karadeniz, Analysis of temperature dependent electrical properties of Au/perylene-diimide/n-Si Schottky diodes, Thin Solid Films 534 (2013) 614–620, http://dx.doi.org/10.1016/j.tsf.2013.02.042.

[33] E.R. Heller, J.P. Pelz, Observation of a scanning tunneling microscopy induced photocurrent during ballistic electron emission microscopy, Appl. Phys. Lett. 82 (2003) 3919, http://dx.doi.org/10.1063/1.1579844.

[34] M.A. Kuikka, W. Li, K.L. Kavanagh, H.-Z. Yu, Nanoscale electrical and structural characterization of gold/alkyl monolayer/silicon diode junctions, J. Phys. Chem. C 112 (2008) 9081–9088, http://dx.doi.org/10.1021/jp802685j.

[35] L. Aversa, R. Verucchi, R. Tatti, F.V. Di Girolamo, M. Barra, F. Ciccullo, et al., Surface doping in T6/PDI-8CN_2 heterostructures investigated by transport and photoemission measurements, Appl. Phys. Lett. 101 (2012) 233504, http://dx.doi.org/10.1063/1.4769345.

[36] D.R.T. Zahn, G.N. Gavrila, M. Gorgoi, The transport gap of organic semiconductors studied using the combination of direct and inverse photoemission, Chem. Phys. 325 (2006) 99–112, http://dx.doi.org/10.1016/j.chemphys.2006.02.003.

[37] P.I. Djurovich, E.I. Mayo, S.R. Forrest, M.E. Thompson, Measurement of the lowest unoccupied molecular orbital energies of molecular organic semiconductors, Org. Electron. 10 (2009) 515–520, http://dx.doi.org/10.1016/j.orgel.2008.12.011.

[38] D. Tsikritzis, S. Kennou, S. Milita, F. Liscio, F. Biscarini, Study of PDI-8CN_2/Au Interface by Photoelectron Spectroscopies, in: Proc. XXVII Panhellenic Conf. Solid State Phys. Mater. Sci., Limassol, Cyprus, 2011, pp. 75–76.

[39] M. Tao, S. Agarwal, D. Udeshi, N. Basit, E. Maldonado, W.P. Kirk, Low Schottky barriers on n-type silicon (001), Appl. Phys. Lett. 83 (2003) 2593, http://dx.doi.org/10.1063/1.1613357.

[40] I.G. Hill, A. Rajagopal, A. Kahn, Y. Hu, Molecular level alignment at organic semiconductor–metal interfaces, Appl. Phys. Lett. 73 (1998) 662, http://dx.doi.org/10.1063/1.121940.

[41] K.S. Lokesh, K. De Wael, A. Adriaens, Self-assembled supramolecular array of polymeric phthalocyanine on gold for the determination of

hydrogen peroxide, Langmuir 26 (2010) 17665–17673, http://dx.doi.org/10.1021/la102740s.
[42] M. Gorgoi, W. Michaelis, T.U. Kampen, D. Schlettwein, D.R.T. Zahn, Thickness dependence of the LUMO position for phthalocyanines on hydrogen passivated silicon (111), Appl. Surf. Sci. 234 (2004) 138–143, http://dx.doi.org/10.1016/j.apsusc.2004.05.065.
[43] J.M. Mativetsky, E. Orgiu, I. Lieberwirth, W. Pisula, P. Samorì, Charge transport over multiple length scales in supramolecular fiber transistors: single fiber versus ensemble performance, Adv. Mater. 26 (2014) 430–435, http://dx.doi.org/10.1002/adma.201303419.